A transparent IHPV for the in-situ geochemical characterization of magmatic volatile phases and melts

Marion Louvel, Denis Testemale, Alain Prat, Eric Lahera, William Del-Net, Aneta Slodczyk, Benjamin Langerome, Rémi Champallier, Richard Brooker, Anita Cadoux, et al.

Journal of Volcanology and Geothermal Research 466 (2025) 108381

Contents lists available at ScienceDirect

Journal of Volcanology and Geothermal Research

journal homepage: www.journals.elsevier.com/journal-of-volcanology-and-geothermal-research

A transparent IHPV for the in-situ geochemical characterization of magmatic volatile phases and melts

Marion Louvel [a,*], Denis Testemale [b], Alain Prat [b], Eric Lahera [b], William Del-Net [b,c], Aneta Slodczyk [a,d], Benjamin Langerome [a], Remi Champallier [a], Richard Brooker [e], Anita Cadoux [f], Jasper Berndt [g], Jean-Louis Hazemann [b]

[a] Institut des Sciences de la Terre d'Orléans, UMR 7327, Univ Orleans-CNRS-BRGM, OSUC, F-45071, Orléans, France
[b] Institut Néel, UPR 2940, Université Grenoble Alpes, CNRS, Grenoble INP, F-38000 Grenoble, France
[c] Laboratoire de Physique Subatomique et Cosmologie, UMR 5821, Université Grenoble Alpes, CNRS, Grenoble INP, F-38000 Grenoble, France
[d] CEMHTI, UPR 3079, CNRS, F-45071 Orléans, France
[e] School of Earth Sciences, University of Bristol, United Kingdom
[f] Harvard John A. Paulson School of Engineering and Applied Sciences, Harvard University, Cambridge, MA, USA
[g] Institut für Mineralogie, Westfälische Wilhelms-Universität, 48148 Münster, Germany

ARTICLE INFO

Keywords:
Degassing
Magmatic-hydrothermal fluids
High-temperature experiments
In-situ measurements
Halogens

ABSTRACT

Chemical exchanges between magmas and volatile-rich fluids and gases are fundamental processes of magmatic and volcanic activity, but also play a critical role in the formation of various ore deposits. Yet, the composition and properties of the so-called magmatic volatile phases (MVPs) remain elusive, due to difficulties in their sampling, both in natural systems and in experimental laboratories.

Here, we present a novel 'transparent' internally-heated high-pressure vessel (T-IHPV) that enables the geochemical characterization of coexisting hydrous melts and MVPs in-situ, under typical shallow magmatic conditions. The experimental design is validated through the observation of haplogranite and rhyodacite melting to 900 °C and 130 MPa and the in-situ X-ray absorption (XAS) study of bromine and strontium distribution and speciation in the haplogranite-H_2O system to 800 °C and 100 MPa. These preliminary experiments confirm the efficient partitioning of Br in MVPs in differentiated systems ($D_{Br}^{MVP/melt}$ around 41 for haplogranite) and reveal the stability of hydrated Br species instead of HBr in the MVPs. Coupled to other spectroscopic methods (Raman, SAXS/WAXS, XRD), we expect the T-IHPV to shed a new light on the thermodynamics and kinetics of chemical reactions at stake in shallow magmatic and hydrothermal reservoirs.

1. Introduction

Magmatic volatile phases or MVPs are key components of crustal magmatic systems. At depth, their exsolution and escape have been associated with changes in the chemical and rheological properties of magmas, with potential impact on the development of volcanic eruptions (Edmonds and Wallace, 2017). In various settings, they are also responsible for the mobilization and economic concentration of metals, including the formation of Cu-Au-Mo porphyry deposits along volcanic arcs (Audetat and Edmonds, 2020). Towards the surface, volcanic gaseous emissions, including that of potentially toxic metals and metalloids (Cd, Se, As, Hg) shape the daily life of local populations but also the past and future evolution of the Earth's atmosphere. As such, MVPs may also carry information about the magmatic component of degassing and the state of the magma reservoir at depth; a better understanding of their properties from depth to surface is thus critical to the monitoring and prediction of volcanic activity (Oppenheimer et al., 2014).

The P-T conditions of MVPs exsolution (i.e., degassing) from magmas have been addressed through the study of volatiles concentrations in melt inclusions (Gennaro et al., 2019; Metrich and Wallace, 2008) and the experimental determination of H_2O-CO_2-S-Cl solubilities in silicate melts (Lesne et al., 2011, 2015; Scaillet and Pichavant, 2005; Signorelli and Carroll, 2002; Webster, 1997; Webster et al., 1999, 2014). While a relatively comprehensive dataset is available for basalts and rhyolites, studies focusing on intermediate composition are scarcer. Furthermore, the evolution of their chemico-physical properties upon decompression,

* Corresponding author.
E-mail address: marion.louvel@cnrs.fr (M. Louvel).

https://doi.org/10.1016/j.jvolgeores.2025.108381
Received 7 February 2025; Received in revised form 22 May 2025; Accepted 26 May 2025
Available online 1 June 2025

cooling and interactions with their surroundings remains poorly understood, mostly because MVPs are scarcely sampled in nature and difficult to produce and recover for conventional geochemical analyses in the laboratory.

Most MVPs produced at $T > 600$–700 °C and $P < 500$ MPa may be considered as supercritical fluids. However, their microscopic properties will deviate more or less from 'liquid-like' to 'gas-like' as a function of P-T conditions and their composition. Here, liquid-like is understood as conditions under which the three-dimensional H bond network of the water-based solvent is still well expressed, whereas 'gas-like' supercritical fluids are constituted of molecular water clusters $(H_2O)_n$. While there is no clear physical limit between those two-domains but instead a continuous change of properties, a rough limit can be placed around a density of 0.3–0.35 g·cm^{-3} for supercritical water-rich fluids (Lemke and Seward, 2018; Pokrovski et al., 2013; Schienbein and Marx, 2020). Thus, while MVPs produced at $T > 900$ °C, $P > 200$ MPa and NaCl > 0.5 m (2.9 wt% $NaCl_{eq}$) that have densities above 0.4 g·cm^{-3} may be classified as 'liquid-like', those with lower Cl contents, containing CO_2, or generated at pressure below 200 MPa (i.e., roughly equivalent to a 6 km depth) will be low density 'gas-like' phases. Decompression-driven phase separation in Cl-rich systems will also form 'gas like' phases with density < 0.2 g·cm^{-3}. Typical volcanic vapors, as sampled at fumarolic vents have densities below 0.1 g·cm^{-3} and will only form under near-surface conditions, below 30–40 MPa (i.e., <1 km depth).

In nature, sampling and analyses of high-temperature volcanic fumaroles only provide 'end-member' information about the composition and properties of MVPs towards the surface with the original magmatic signature potentially distorted by decompression, cooling or chemical interactions between the MVPs and surrounding rocks, hydrothermal systems or air (Chiodini et al., 2017; Henley and Seward, 2018; Moretti et al., 2013). For instance, part of the elements that were volatile at depth, including some metals, may sublimate as halides, sulphides or sulfate minerals on their way to surface. At depth, MVPs trapped as fluid inclusions suggest they may contain from 70 to 90 wt% H_2O, and varying amounts of CO_2, (H, Na, K)Cl, H_2S or SO_2 depending on their source and P-T conditions of formation (Audetat and Edmonds, 2020; Pokrovski et al., 2013; Williams-Jones and Heinrich, 2005). However, reconstruction of their conditions of entrapment and high P-T composition from microthermobarometry may be difficult for complex compositions that not only include H_2O, CO_2 and NaCl but also high amounts of H_2S, SO_2 or other solutes (e.g., KCl, $FeCl_2$). Furthermore, fluid inclusions may also be subject to chemical reequilibration through time or interaction with external fluids (Mavrogenes and Bodnar, 1994; Zajacz et al., 2009; Guo and Audetat, 2018).

Over the last 30 years, different experimental strategies have thus been put in place to overcome the complexity of natural samples and investigate MVPs equilibrated with melts under typical crustal magmatic conditions ($600 < T < 1300$ °C and $P < 500$ MPa) directly in the laboratory. The main aim of these experiments is to constrain the nature, stability and distribution of chemical species between MVPs and melts, in the hope to build an empirical database for the modelling of ore-forming processes or volcanic degassing. Such experimental constraints may also come as a support for theoretical calculations of gas properties already implemented in different numerical codes (e.g., GEM-Selektor, Gastherm or D-Compress; Burgisser et al., 2015; Symonds and Reed, 1993; Hurtig et al., 2021). After a brief review of these techniques, their advantages and drawbacks, we here present a new device developed conjointly by the Institut Néel (Grenoble, France) and the Institut des Sciences de la Terre d'Orléans (ISTO, Orléans, France) to study in-situ coexisting water-saturated melts and MVPs under shallow magmatic conditions. The capabilities of the experimental set-up in term of achievable P-T conditions, containment of the volatile-rich phase and the in-situ characterization of trace elements are tested via an X-ray absorption (XAS) investigation at the Br and Sr energy K-edges. The in-situ XAS also carry preliminary information about Br and Sr speciation and distribution in the haplogranite-H_2O system.

2. The laboratory study of MVPs: scientific advances and technical limitations

A key issue with the experimental study of high P-T geological fluids is that their chemico-physical properties are often not quenchable to room conditions. This includes high amounts of dissolved species that will precipitate upon quench or chemical complexes and trace element oxidation states that are only stable above a certain temperature. High P-T fluids may also react with the sample containers or change their tensile properties, resulting in the loss of some elements to the capsule material or shortened lifetime of the experimental apparatus. To overcome these issues, different approaches have been employed, relying either on the *post-mortem* reconstruction of high P-T properties through careful analysis of quenched materials or on the in-situ analysis of the samples. Our main interest being in the processes of magmatic exsolution or degassing, we mostly report on the approaches that make use of experimental tools that enable melting of silicate glasses under hydrous conditions, i.e., temperature conditions above 600 °C. A summary of different techniques, along with their achievable P-T conditions, possibility of fugacity control, sample size, analytical techniques and results obtained can be found in Table 1. They are further detailed in the next paragraphs.

2.1. Volatilization from high-T oxides and melts under low pressures (<20 MPa)

Currently, the larger dataset available on the properties of low-density gas species is probably built upon low-pressure experiments that allow for either recovery of condensed vapour or direct analysis of the gas phase through coupling of flow-through cells with high-temperature mass-spectrometer (Pokrovski et al., 2013). A large number of available data have been obtained in the scientific context of industrial applications or outgassing of terrestrial exoplanets and vaporisation in the solar nebula (Meschter et al., 2013; Myers and Jacobson, 2019; Thompson et al., 2021). Therefore, most techniques focus on vacuum to 1 bar vapour pressure and detailed description of the coupling of high T (>1000 °C) furnaces and flow through cells with Knudsen effusion (KEMS), Free Jet Expansion Sampling (FLESMS) or residual gas analyzer (RGA) mass spectrometers is deemed beyond the scope of this paper. Similarly, most condensation experiments, using 'transpiration techniques' only allow for atmospheric pressure (e.g., Hashimoto, 1992).

Few vapour deposition studies however make use of large evacuated silica tubes (Ø 4–5 mm, length up to 30 cm) that are placed in a 1 atm furnace with a vertical temperature gradient (e.g. from 1250 to 300 °C) and allow for saturated vapour pressures of few bars that may apply to surface degassing of lavas and reproduce the precipitation of metals and minerals upon magmatic degassing of exoplanets or at fumarolic vents (e.g., Nekvasil et al., 2019; Renggli and Klemme, 2020). Starting materials may include oxides or silicate glasses that are placed in the hot zone of the furnace. New solid phases deposited along the silica tubes are recovered post-quench, and can be quantitatively characterized through various destructive (LA-ICPMS) and non-destructive techniques (Raman, FTIR, SIMS). The gas phase is however lost upon opening the silica tubes and its composition may only be derived from balancing chemical reactions and thermodynamic modelling. Furthermore, the use of silica tubes as the sample holder limits the range of gas composition that may be investigated to anhydrous conditions due to silica dissolution at high temperatures.

2.2. The mass balance approach and rapid quench/large volume internally-heated pressure vessels

Large volume internally-heated pressure vessels (IHPV) were first introduced in details by Burnham (Burnham and Jahns, 1962; Burnham et al., 1969). They consist of a resistive furnace surrounding a large

Table 1
The different experimental approaches used to characterize the composition and properties of magmatic volatile phases.

Apparatus[a]	P-T_{max}	fO_2 controls	Sample size/ volume	Experimental timescales	Geochemical analyses[b]	Information obtained	Selected references[c]
Volatilization experiments							
1 atm furnaces	800 < *T* < 1800 °C 1 atm < *P* < 20 MPa	Gas mixtures (CO, CO_2, SO_2, H_2S, Ar, O_2, H_2, N_2, Cl_2)	Several cm^3	Up to few days	SEM, Raman, EPMA, LA-ICPMS, etc.	• Post-mortem characterization of solids. • Gas composition is calculated from available thermodynamic models.	1, 2,3,4
Mass balance calculations							
IHPV (CS, PC)	800 < T < 1300 °C 100 < *P* < 1000 MPa	P_{H2} measured (H_2-membrane)	Up to 4 cm^3	Few days to weeks	SEM, Raman, EPMA, LA-ICPMS, etc.	• Post-mortem characterization of solids. • MVP composition is back-calculated. *May be complemented by the analysis of quenched fluids after careful cleaning procedures.*	5,6,7
Entrapment in SFLINCS							
CS (PC)	700 < *T* < 1200 °C 100 < P < 500 MPa	Imposed by capsule design or gas mix	SFLINCS are 10–100 s μm	24 h to few days	SEM, Raman, EPMA, LA-ICPMS, etc.	• Post-mortem characterization of solids and fluids.	8,9,10
In-situ spectroscopy in HDAC							
HDAC	25 < *T* < 1000 °C 300 < *P* < 7000 MPa	Unknown. Affected by a combination of gasket material (Re), graphitization of diamonds at extreme T and the flushing of Ar-H_2 gas mixture. *Possibility to use Ir gaskets and flush Ar + CH_4 or load an internal mineral buffer to vary redox.*	Up to 0.02 mm^3	From 2 to 10–12 h	XAS, SXRF, XRD or Raman	• In-situ chemical and structural characterization of fluids and melts. • Quenched glasses may be recovered for post-mortem analysis.	11,12,13,14
In-situ spectroscopy in transparent IHPV – this study							
PLANEX autoclave	25 < T < 1200 °C 1 < *P* < 200 MPa	Unknown. Probably C-CO at T > 600 °C with vitreous carbon cells. *Possibility to use sapphire cells and load an internal mineral buffer to vary redox. Pressuring gas (He) cannot be changed.*	Up to 80 mm^3	From 2 to 10–12 h	XAS or Raman	• In-situ chemical and structural characterization of fluids and melts. • Quenched glasses may be recovered for post-mortem analysis.	

[a] IHPV = internally-heated pressure vessel; CS = cold-seal pressure vessels; PC = piston cylinders; HDAC = hydrothermal diamond-anvil cells.
[b] Techniques for geochemical analyses: SEM: Scanning electron microprobe; EPMA: Electron probe microanalyzer; LA-ICP-MS: laser-ablation inductively coupled plasma mass spectrometer; FTIR: Fourier transform infrared; XAS: X-ray absorption spectroscopy; SXRF: synchrotron X-ray fluorescence; XRD: X-ray diffraction.
[c] [1] Gooding and Muenow, 1976. [2] Thompson et al., 2021. [3] Nekvasil et al., 2019. [4] Renggli and Klemme, 2020. [5] Burnham, 1962. [6] Scaillet et al., 1992. [7] Gion et al., 2022. [8] Sterner and Bodnar, 1984. [9] Zajacz et al., 2010. [10] Alex and Zajacz, 2020. [11] Bassett et al., 1993. [12] Mysen, 2010. [13] Louvel et al., 2020a.[14] Schmidt, 2018.

sample chamber and placed within a (water-cooled) pressure vessel. Pressure is transmitted to the samples through Ar gas injected in the high-pressure vessel, enabling a precision within 0.2 MPa. The samples are contained in large (e.g., diameter Ø up to 1 cm and length up to 5 cm) welded noble metal capsules and most designs allow for the loading of several capsules within the sample chamber. A review of IHPV designs and capabilities can be found in Holloway (1971) and several contributions also presented updates and improvements for rapid quench (100–200 °C/s) or fO_2 control (e.g., Holloway et al., 1992; Scaillet et al., 1992; Berndt et al., 2002). Typically, IHPV can be used to T_{max} = 1400 °C and P_{max} = 500–700 MPa for several hours to weeks, thus allowing for the melting of rhyolitic to basaltic compositions and the study of volatiles behaviour from relatively deep magmatic intrusions or magma chambers. Over the years, IHPV have mostly been used to assess the solubility of volatiles in silicate and even carbonate melts over a wide range of P-T-fO_2 conditions (e.g., Botcharnikov et al., 2005; Holtz et al., 1995; Keppler et al., 2022; Lesne et al., 2011, 2015; Moussallam et al., 2015; Scaillet and Pichavant, 2005; Webster et al., 1999) and thus provide constraints on the conditions of MVPs exsolution. However, several laboratories also used them to assess the actual composition of coexisting MVPs and melts to constrain fluid-melt partition coefficients for volatiles (S, Cl, Br) or trace elements (Li, Cu, Zn, Rb, Sr, Mo, W, etc.) (Alletti et al., 2009; Cadoux et al., 2018; Iveson et al., 2017, 2019; Webster and Holloway, 1988; Webster et al., 1989, 2009, 2014; Webster, 1992). Note that some laboratories have also made use of cold-seal pressure vessels and piston-cylinders to constrain MVP/melt partitioning of volatiles and metals (e.g., Zajacz, 2015; Zajacz et al., 2012). As quenching of the high P-T capsules leads to solute precipitation from the MVPs, these experiments usually rely on the quantitative analysis of the quenched glasses and mass balance calculations to estimate the high P-T composition of fluids/gases. This approach requires precise weighing of the starting materials, quenched and dried capsules. The fluid phase may also be recovered after careful sampling of all potential fluid precipitates to be analysed post-quench (e.g., chloridometry or ICP-MS - Iveson et al., 2017, 2019; Gion et al., 2022), and usually allow for similar estimations as with the mass balance approach.

A main limitation of mass balance experiments however lies in the identification of potential phase separation of the MVP that may occur under high P-T conditions or upon quench and its bearing on mass balance calculations of partition coefficients. While the P-T conditions of

brine-vapour separation are for instance well mapped for the binary H_2O-NaCl system (Driesner, 2007), little is known about the effects of CO_2 and S on this transition. The presence of S may be considered even more of a hindrance when taking into account the potential loss of SO_2 and H_2S upon puncturing of the capsule, the precipitation of S-bearing minerals at high P-T or upon quench or S incorporation into capsule material that can all complicate the mass balance calculations (see Webster and Botcharnikov, 2011 and references therein). The same is true for metals that may form alloys with the capsule materials (e.g., Cu or Mo) or complications arising from the precipitation of other poorly-soluble phases, such as fluorides or aluminosilicates. Comprehensive discussions of the calculations and associated uncertainties can be found in Webster and Holloway (1988), Cadoux et al. (2018) or Iveson et al. (2019).

Finally, the nature of the chemical species stable under high P-T conditions remains the biggest unknown of the mass balance approach. Further modelling of the effects of P-T conditions and composition on the ongoing chemical exchange between MVPs and melts thus mostly rely on 1) the knowledge of element speciation in quenched glasses and silicate melts, for instance constrained via Raman, FTIR, XAS or NMR spectroscopy (e.g., Wilke et al., 2011 or Ni and Keppler, 2013 for S and C species), and 2) theoretical modelling of solvated gas species for the fluid phase (Lemke and Seward, 2018; Pokrovski et al., 2013).

2.3. SFLINCs and cold-seal pressure vessels

In parallel to the mass balance reconstructive approach, other laboratories focused on designing experimental set-up that enables the entrapment of the MVPs as synthetic fluid inclusions (SFLINCs) (Sterner and Bodnar, 1984; Lecumberri-Sanchez et al., 2020; Zajacz et al., 2010). This approach generally makes use of cold-seal pressure vessels that enable pressure and temperature conditions in the 100–500 MPa and 700–1200 °C range, although SFLINCS have also been synthesized in IHPV or under higher pressure conditions in piston cylinder apparatus (e.g., Hack and Mavrogenes, 2006). High P-T fluids are trapped through the healing of fractures of large quartz crystals (e.g., Ø 0.5–1 cm, length 1–2 cm) loaded together with a solution of known composition in a noble metal capsule. In the case of cold-seal pressure vessels, several capsules can be placed together in hot part of the pressure vessel, which is a 30–40 cm long alloy 'bomb' connected to a water or gas pressure system. The use of gas mixture as Ar-CH4 or Ar-H2 allows for controlled gas atmosphere in some apparatus (Alex and Zajacz, 2020). The bomb is heated externally by being placed in a furnace through a manual or (faster) motorized system. Fracturing is accomplished either before the experiment, by subjecting the quartz crystals to thermal shock, or in-situ, in devices where it is possible to rapidly remove and replace the bomb inside the furnace (e.g., Zajacz et al., 2010). It is worth noting that cold-seal pressure vessels made from Ni-rich alloys generally have a limited lifetime when used to temperatures above 700–800 °C. Different Mo-rich alloys may be used to reach high temperatures, but a general rule of thumb is that increasing pressure and temperature shortens the bomb lifetime. Further information on different designs and discussions about the capabilities of different alloys or the use of fugacity controls can be found in Luth and Tuttle (1949), William (1968) or more recently Alex and Zajacz (2020).

As mass balance calculations, SFLINCs offer great capabilities for chemical quantification of the MVPs. The main advantage of the technique is that the fluids are trapped in-situ during the experiments and hence sample the high P-T composition accurately. Cl, but also CO2/CH4 contents in the quenched MVPs can be quantified via microthermometry. The SFLINCs are also amenable to various spectroscopic techniques, including Raman and LA-ICPMS that enable quantification of trace elements or of certain volatiles (C or S species). SFLINCs have consequently been used to study the phase stability (vapour ± liquids, halides) and PVTX properties of H2O-NaCl±KCl,CH4,CO2, fluids trapped in quartz crystals (Sterner and Bodnar, 1984; Lecumberri-Sanchez et al., 2020) or the solubility or the vapour/brine and MVP/melt partitioning of chlorine, trace elements and various metals (Li, B, Rb, Sr, Cu, Zn, Au, Mo, Sb, Te, etc.) under a large range of P-T-fO2/fS2 ± CO2 conditions (Frank et al., 2011; Guo and Audetat, 2017; Simon et al., 2005; Tattitch and Blundy, 2017; Tattitch et al., 2014, 2021; Zajacz et al., 2010; Zajacz et al., 2012, 2017).

An important limitation of this method however lies in the use of quartz, which not only imposes quartz-saturated conditions on the experiments but more critically prevents the study of highly reactive systems such as those involving F-rich fluids or carbonatite melts. Also, SFLINCs analysis with LA-ICPMS requires the access to a source that enables controlled ablation of the small inclusions (e.g., ArF (193 nm) Excimer laser system with beam-homogenising optics - Heinrich et al., 2003). As for mass balance calculations, the actual nature of the MVP under high P-T conditions (i.e., whether it is a single fluid phase or brine+vapour) may be difficult to constrain for complex fluid containing CO2 or S, and capsule design is of critical importance to avoid loss of S or certain metals to the capsule (Zajacz et al., 2012; Tattitch and Blundy, 2017).

While direct information about volatiles or trace element speciation in the MVPs is lost upon quench to room conditions, solubility and fluid-melt partitioning constraints from SFLINCs have been used to estimate the dominant chloride and sulphide Cu or Au species stable in MVPs, based on the relationship between metal solubility and Cl contents or fH2S (e.g., Zajacz et al., 2010; Tattitch and Blundy, 2017). Similar information describing the nature of complexes with Cl and S ligands and their degree of solvation can be found for many other metals from solubility experiments in low-density fluids in hydrothermal reactors (Pokrovski et al., 2013; Williams-Jones and Heinrich, 2005). However, those are mostly limited to $T < 500$ °C and whether the proposed structures are stable to magmatic conditions remains a matter of debate. These models also require initial assumptions about the redox state of metals and trace elements that are sometimes disproven by in-situ spectroscopic analyses (see the examples of Au and Cu and the detailed discussion provided for hydrothermal studies in Pokrovski et al., 2013).

2.4. In-situ measurements in optical cells

It transpires from the above that while most techniques relying on quench or entrapment of high P-T phases may be well suited to the quantitative evaluation of chemical exchanges between MVPs and melts, none of these approaches enables the molecular description of the species stable in the MVPs that is necessary to the development of adequate thermodynamic models. In-situ approaches, which make use of high-pressure windows transparent to different light sources, may help to overcome this limitation and enable characterization of both concentration and speciation in high P-T fluids and melts at equilibrium. The development of such devices is however more recent and still limited. For instance, while the hydrothermal autoclave of Testemale et al. (2005) or fused silica capillaries capsules (FSCCs – Chou, 2012) have been used to study the transport capacities of low-density fluids via Raman or XAS spectroscopy (Caumon et al., 2014; Etschmann et al., 2010; Louvel et al., 2017; Pokrovski et al., 2013), maximum achievable temperature conditions are curbed below 500–600 °C. The Bassett-type hydrothermal diamond-anvil cell (HDAC) and its derivatives are, to the best of our knowledge, the only high-pressure optical cells that enable reaching 'magmatic' temperature conditions, up to about 1000 °C (Bassett, 2003; Li et al., 2016; Louvel et al., 2020a). In-situ determination of the sample pressure however remains problematic, with large uncertainties for $P < 1$GPa, and few studies thus reported in-situ Raman or XAS measurements under typical crustal magmatic conditions in HDAC (e.g., Borchert et al., 2009, 2014; Louvel et al., 2014). Furthermore, the fO2 conditions potentially imposed by the competitive oxidation of diamond anvils and gasket material (Re) by the MVPs at $T > 600$ °C are currently unconstrained, with only one study investigating

fO2 conditions in the HDAC to a maximum temperature of 500 °C (Solferino and Anderson, 2012). Furthermore, the recourse to diamond anvils to generate pressure results in small sample size (sample chamber containing fluid+melt are generally <500 μm) and thus requires access to microanalysis facilities, such as micro-XAS beamlines at synchrotron sources. Therefore, the HDAC remains better adapted to the study of deep geological fluids formed in the lower crust or the subducting slab.

3. In-situ experiments in the transparent IHPV

3.1. Technical implementation

The T-IHPV consists of a 340 × 150 cm^2 water-cooled high-pressure vessel equipped with three 4.5 mm thick Be high-pressure windows (Fig. 1A), whose original design (Testemale et al., 2005) was adapted for increased stability and optimal heat conservation to 1200 °C and 200 MPa. It is, by essence, a small IHPV that can be easily transported to different facilities for in-situ spectroscopic analyses. The sample is contained in a 10 cm long vitreous C sample cell (internal diameter 5 mm), closed by two vitreous C pistons equipped with Viton or Silicon O-rings for hermetical sealing (Fig. 1B).

Compared to the original design, which operated routinely to 500 °C and 200 MPa, the position of the sample tube in the autoclave and the geometry and nature of insulating ceramics were optimized to improve the thermal insulation of the sample. He gas is delivered through the side of the high-pressure body (Fig. 1A), for better adaptability of the high-pressure vessel on the X-ray beam path for XAS measurements. The pressure inside the T-IHPV is regulated to around 0.2 bar by a dedicated system of electrovalves (Bruyere et al., 2008; now commercialized by Maximator, France). The heating element consist of a roughly 60 cm long and 0.4 mm diameter Mo wire that is wrapped around a 30 mm long Mo cylinder that surrounds the vitreous C sample cell, with the ~2–3 mm thick sample (melt+fluid) placed at the centre of the Mo cylinder (Fig. 1). The wire is further isolated by alumina ceramic tubes and Cotronics® HT940 ceramic bond. Three 25 μm thick Be foil screens are also placed between the ceramics and the spectroscopic windows of the vessel so that convective temperature loss is minimized. Temperature is read by two K-type thermocouples placed within the Mo cylinder. The offset between the temperature read by the thermocouples and the actual temperature of the sample in the vitreous carbon cell is calibrated at the beginning of the experiment by measuring the density of pure H2O in the sample cell over the investigated P-T range (Louvel et al., 2017). Temperature offset is generally below 25 °C for $T < 500–600$ °C (e.g., Guan et al., 2020; Louvel et al., 2017). For the current experiments, we observed an offset of about 100 °C at 800 °C and 100 MPa. There is no vertical temperature gradient within the sample, as evidenced by flat transmission profiles for the MVP (see Fig. 3 for an example at 800 °C and 100 MPa).

The internal design of the sample cell was also optimized for the study of coexisting hydrous melts and fluids/gases. Silicate glasses are loaded as 1.5 mm diameter beads in a 2 mm long and 1.7 mm diameter recess in the lower piston to prevent hydrous melts flowing along the vitreous C pistons at high P-T conditions and ensure that data are collected from either pure fluid or pure melt phases (Fig. 1B). Then, the cell is filled with a weighed amount of H_2O or aqueous solution. The aqueous and glass samples are pressurized under room temperature. As temperature is increased, the lower piston is kept at a fixed position in the experimental design by adding a ceramic spacer that prevents its movement, ensuring that the melt sample remains in the spectroscopic windows at all time. Meanwhile, the upper piston can move freely along the sample tube to accommodate volume change upon isobaric temperature increase.

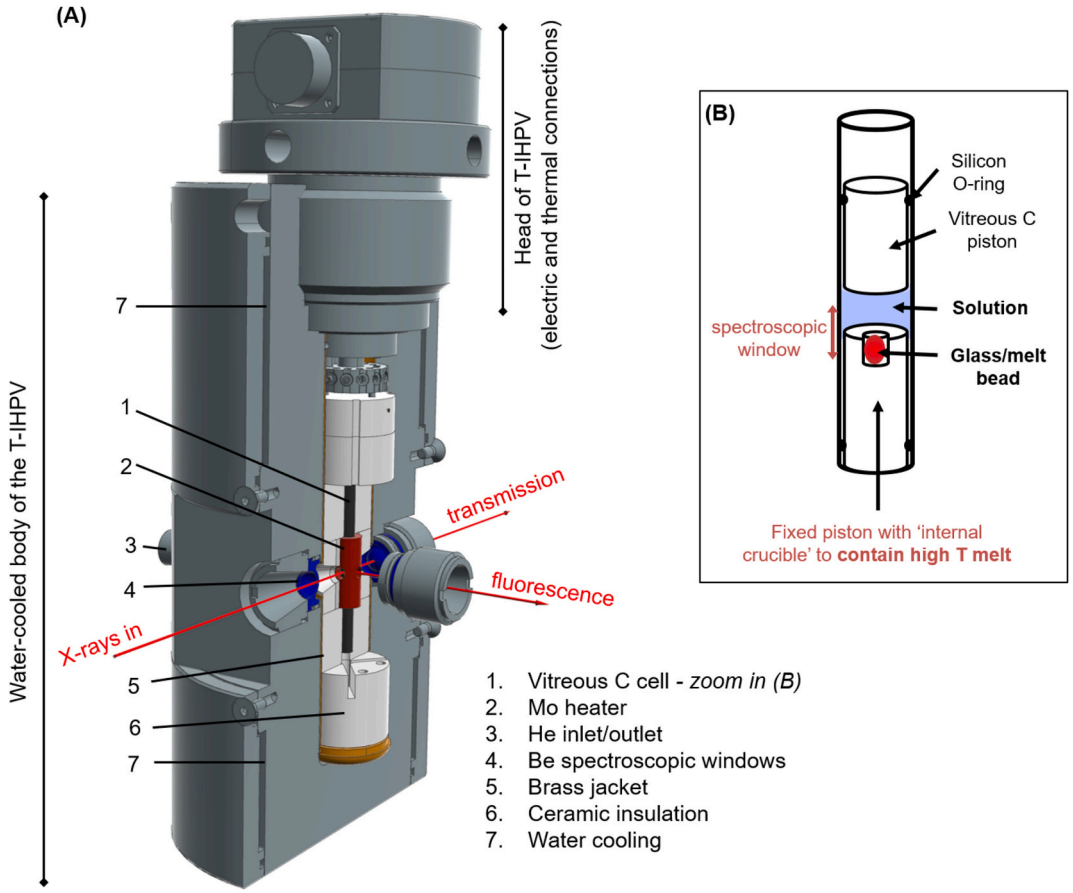

Fig. 1. Schematic view of the T-IHPV (A) and sample loading (B).

3.2. *In-situ XAS measurements in the transparent IHPV: test experiments and beamline specifics*

The new design and capabilities of the T-IHPV to study MVP properties have been tested using in-situ XAS measurements at the BM-30B beamline at European Synchrotron Radiation Facility ESRF (Proux et al., 2005). We chose to study Br, an element that has an ideal mass and sufficiently strong affinity for the fluid phase to ensure high concentration for in-situ measurements. Br is of particular interest as it is frequently used as an analog for more common Cl, which is not amenable to in-situ technics due to low-energy of excitation. Furthermore, Br degassing has been a subject of matter, due to its significant impact on the atmosphere (Von Glasow et al., 2009). Finally, Br fluid-melt partitioning and speciation in both fluids and melts are overall well-known (Bureau et al., 2000; Cadoux et al., 2018; Louvel et al., 2020a, 2020b), providing a benchmark for our experiments. In order to test the capabilities of the T-IHPV for in-situ measurements on hydrous melts, we also study Sr, which is known for its low fluid-melt partition coefficients (Borchert et al., 2010) and has a K-edge sufficiently close to that of Br to enable alternate XAS analysis of both elements within a single loading.

The high P-T behaviour of Br and Sr were studied in five different systems: Load 1 consisted of a Br-bearing solution (~8500 ppm) prepared from deionized water and NaBr powder (Sigma-Aldrich) loaded in the sample tube to test for potential high T leakage and validate the quantification procedure for Br in MVPs; Load 2 involved a Br-doped (3400 ppm) haplogranite glass (Hpg_ML5) loaded with the Br-bearing solution; Loads 3 and 4, a Br-free and Sr-doped (1000 ppm)

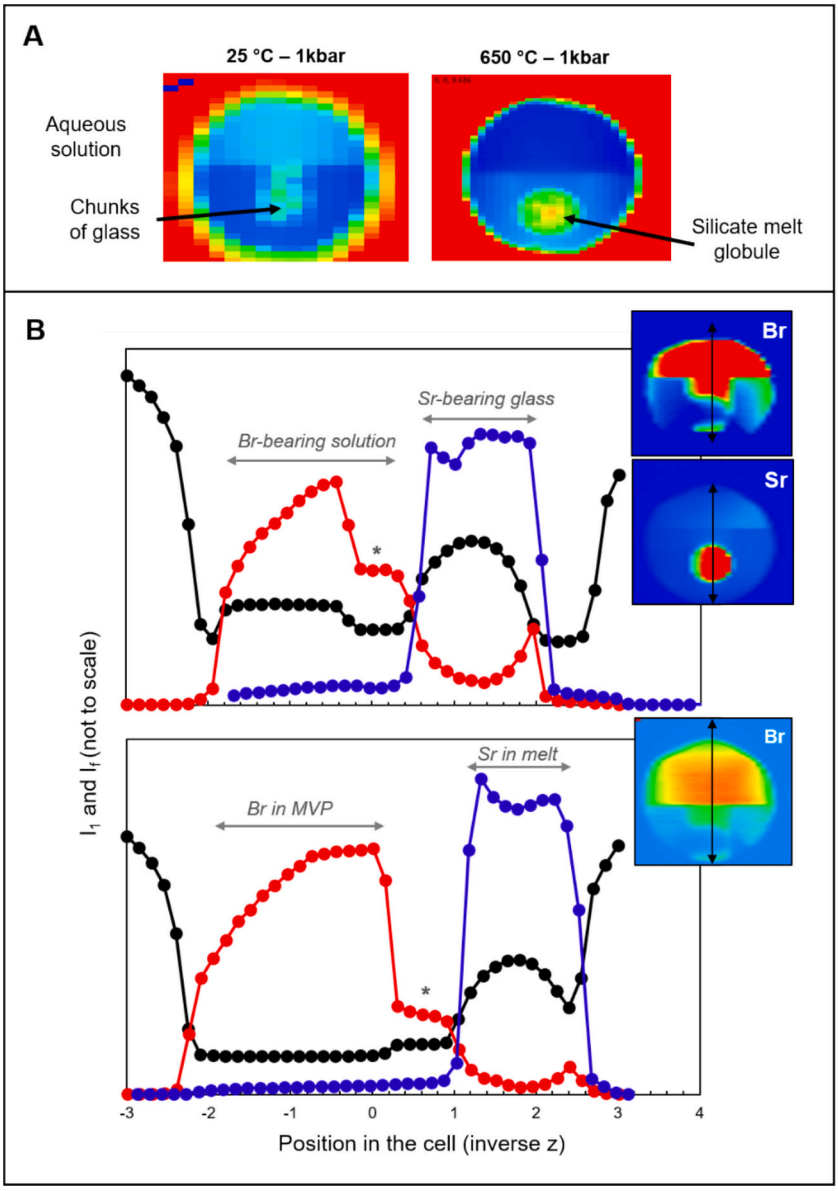

Fig. 2. (A) Example of 2D maps collected in transmission mode showing the contrast of absorption between aqueous fluid/silicate glass, MVP/melt and vitreous C piston at 25 vs. 650 °C and 100 MPa (Load 2 – Hpg_ML5 + NaBr sol.). The initial solution and high P-T magmatic volatile phase are easily distinguished from the lower piston and the silicate glass/melt through density recorded in the absorption signal: blue colors correspond to the least absorbing materials, i.e., vitreous C cell and piston ± aqueous solution or MVP; glass and melt, which have a higher density and hence absorption than the MVP appear in green to yellow; red delimits the body of the IHPV that blocks all signal. Melting is evidenced by a change from rough edges of glass chips at room temperature to a rounded melt globule at higher T. (B) Throughout the experiments, vertical scans of the X-ray absorption (black lines), Br and Sr fluorescence (red and blue lines, respectively) are collected together with 2D maps to select the position of analysis for the solution/MVP or the glass/melt. * underlines the presence of an air bubble at the bottom of the solution that is evidenced by lower absorption. (For interpretation of the references to color in this figure legend, the reader is referred to the web version of this article.)

haplogranite glass (Hpg_ML4) loaded with the Br-bearing solution; and Load 5 a water-rich (4.75 wt%) and Br-bearing (500 ppm) rhyodacite (RD500_AC) loaded with pure H_2O. Details about the starting materials synthesis and composition can be found in the Supplementary materials.

X-ray Absorption (XAS) spectra were collected alternatively over the Br (13,474 eV) and Sr (16,105 eV) K-edge using a crystal Si(220) monochromator and a beam focused down to 220 × 120 μm^2 (H × V at FWHM) with the 6.03 GeV ring operating in 7/8 multibunches mode at 200 mA. The incident (I_0) and transmitted (I_1) beam intensities were measured with Si diodes, while a Canberra 30 element solid state fluorescence detector was used to collect fluorescence signal (I_f). The beam energy was calibrated and then monitored throughout the experiments from a Se crystalline standard, with the maximum of the first derivative at 12.658 keV.

3.3. Reliability of the set-up at melting conditions (T > 600 °C)

In our test experiments, temperature was increased at a rate of 10 °C/min directly to 650 or 800 °C. The maximum temperature achieved with the new experimental design is 900 °C at 100–130 MPa. These conditions enabled the hydrous melting of the haplogranite and rhyodacite glass samples, as evidenced by recovered quenched glasses that show 1) numerous bubbles attesting of the molten state of the samples or 2) homogeneous major elements contents from electron microprobe analyses (EPMA) (Figs. S1, S2 and Table S1 respectively in Supplementary materials). The hydrous melting was also monitored in-situ, recording modifications in the shape of several glass chunks via vertical absorption profiles and 2-D X-ray absorption maps collected across the sample chamber, as exemplified in Fig. 2A–B.

In the current design, the O-rings that ensure the proper sealing of the sample chamber and the aqueous/gaseous samples are located outside the heating element. Yet, they may become exposed to temperature >230 °C where they are less resistant due to thermal convection in the IHPV body. Thus, experiments were systematically checked for potential leakage of the volatile-rich phase under high pressure and high temperature conditions. To do so, the density of the MVP was calculated from the Beer-Lambert law, using the measured absorption of the sample at 13400 eV (i.e., before the Br K-edge), its calculated attenuation length (assuming a pure H_2O composition) and the X-ray path length through the sample (5 mm). The calculated densities for our MVPs can then be compared to the NIST values for pure H_2O (Wagner and Pruss, 2002) over time. Any deviation larger than 0.05–0.06 g·cm^{-3} compare to the density of pure water at investigated P-T was considered as a leak of the high *P-T* seal that could cause precipitation of the volatile elements or recrystallization of the melt and the experiments were consequently discarded. For the pure NaBr solution, we report calculated densities that are within 1 to 8 % from that of pure H_2O for over 9 h at 650 °C and 100 MPa (0.286–0.332 g·cm^{-3} for our solution versus 0.321 g·cm^{-3} for pure H_2O) (Fig. 3).

Over the five experimental runs, two ended with leakage of the MVPs due to failure of the Viton O-rings: Load 2 (Hpg_ML5 + NaBr sol.), and Load 5 (RD500_AC + H_2O). The high P-T leakage of the MVPs was also associated with high T fragmentation of the melt, evidenced both by expansion of the melt monitored by in-situ 2D absorption maps and numerous and large bubbles in the quenched globules (Figs. S1 and S2 in Supplementary materials). For Loads 3 and 4 (Hpg_ML4 + NaBr sol.), we observed density within 0.05 g·cm^{-3} of the expected NIST values for pure H_2O over periods of 1–2 h at 650 and 800 °C.

3.4. Determination of element concentration and speciation from XAS spectra

XAS spectra collected in transmission mode were used to calculate the elemental concentration of Br and Sr in MVPs and melts following the approach previously described in Louvel et al. (2015, 2017): the method links the high P-T concentration of the analysed elements to the amplitude of the absorption edge Δ(μx) and the sample high P-T density with an estimated uncertainty due to spectral resolution below 5 %. For MVPs, the high P-T density was assumed to be that of pure H_2O from the NIST database (Wagner and Pruss, 2002). For melts, we used the relationships defined by Ochs and Lange (1999) for hydrated silicate melts.

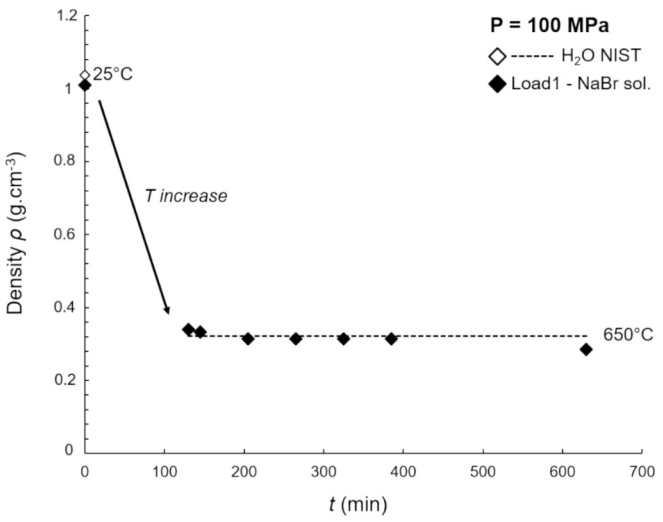

Fig. 3. High P-T density of experimental MVP compared to that of pure H_2O for a NaBr solution (Load 1 - no melt).

XAS spectra collected in fluorescence mode were also used to derive information about Br and Sr speciation in the MVPs and haplogranite melt. For each element, 2 to 7 spectra collected on the MVPs or melt at a given P-T condition were merged together using the Athena software (Ravel and Newville, 2005). The averaged spectra were then normalized to the absorption edge height and the background removed using the subtraction routine AUTOBK available in Athena. The absorption edge E_0 was set at the maxima of the absorption edge first derivative (13,477–13,478 eV for Br; 16,111–16,112 eV for Sr). The X-ray absorption Near-Edge Structure (XANES) part of the spectra (±100 eV above the absorption edge) were then compared to previous data for Br in aqueous fluids and gases (D'Angelo et al., 1993; Louvel et al., 2020a) or Sr in haplogranite glasses and melts (Borchert et al., 2014). When possible (i.e., when the concentration of the element exceeded 1000 ppm in the analysed phase), the Extended X-ray Absorption Fine Structure (EXAFS) spectra were fitted to the EXAFS equation using the Artemis software (Ravel and Newville, 2005) to assess the local structure around the selected atoms (nature and number of nearest neighbors, distance to the central atom). Details about the fitting procedure used for Sr in haplogranite glass and melt can be found in the supplementary materials.

4. Preliminary results on Br and Sr magmatic degassing

4.1. Br in the haplogranite-MVP system

XAS measurements on the Br starting solution at room conditions conducted over 3 different experimental runs (Loads 1, 3 and 4) show an initial Br concentration of 8650 ± 92 ppm, close to the calculated 8500 ppm Br of the prepared solution. Increasing pressure and temperature to MVP conditions does not cause significant precipitation of the Br, as supported by time series of Br concentration in Load 1 that show that an average of 8400 ± 324 ppm Br remains for more than 8 h in the low-density volatile phase at 650 °C and 100 MPa (Fig. S3 in Supp. Mat.). The variability in the calculated Br concentration is within 3–4 % over this entire time, confirming the high P-T sealing of the volatile sample already suggested by density calculations (Fig. 4). Close Br

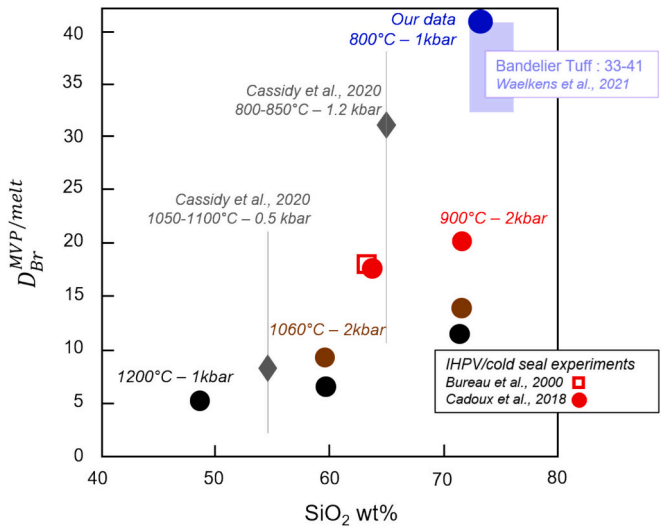

Fig. 4. Comparison of $D_{Br}^{MVP/melt}$ as a function of the melt SiO_2 contents from available experiments (Bureau et al., 2000; Cadoux et al., 2018; Cassidy et al., 2022; this study) and natural estimates (Waelkens et al., 2021). The color code underlines the effect of decreasing temperature on $D_{Br}^{MVP/melt}$.

concentrations are found in the MVP equilibrated with haplogranite melts melt for 1-2 h at the same P-T conditions (8184 ± 66 ppm Br – Load 3) and at 800 °C (7897 ± 368 ppm Br – Load 4).

Unfortunately, the Br concentration in the high P-T melts was too low to enable the collection of transmitted signal necessary for Br in-situ quantification. Instead, the melt globule quenched from 800 °C (Load 4) was recovered and analysed by EPMA following the method described by Flematakis et al. (2020) to account for spectral interference between the Al and Br fluorescence lines (see Supplementary materials for further description). The EPMA measurements suggest that an average of 192 ± 60 ppm Br was present in the haplogranite melt at the glass transition. This concentration translates into a partition coefficient $D_{Br}^{MVP/melt}$ of 41.1 ± 12.3 for haplogranitic melts at 800 °C and 100 MPa, a value that compares favourably with the few experiments available for rhyodacitic ($D_{Br}^{MVP/melt} = 20.2 \pm 1.2$) and albitic ($D_{Br}^{MVP/melt} = 17.5 \pm 0.6$) compositions at 900 °C and 200 MPa (Bureau et al., 2000; Cadoux et al., 2018) and recent estimates made for the Bandelier Tuff (New Mexico, USA) (Waelkens et al., 2021), whose initial melt composition and P-T conditions of degassing were probably closer to our experimental conditions (Fig. 4). Altogether, these data confirm that increased differentiation (increasing SiO_2 contents) and lower temperature of degassing will result in higher $D_{Br}^{MVP/melt}$ and hence promote a more efficient transfer of Br to the atmosphere, with potentially critical effects on the ozone integrity (Von Glasow et al., 2009). The good agreement with previous studies further support that equilibrium was reached in our experiments. Yet, we acknowledge that we here only rely on one experiment and aim to conduct reverse experiments in the future.

The high *P-T* XAS spectra also carry information about Br speciation in the MVP. Br in the MVPs (as in Loads 1, 3 and 4) is characterized by a small white line that peaks at 13482 eV, followed by a shoulder around 13,500 eV (features A and B, Fig. 5). As previously reported for Br in diluted solutions (e.g., Louvel et al., 2020a), the EXAFS part of the spectra is rather featureless at high temperature and it is consequently not possible to derive structural parameters describing the local environment around Br (e.g., number and nature of nearest-neighbors, distance between Br and nearest-neighbors). However, the nature of the Br species can be estimated qualitatively, comparing the XANES spectra to previous data on Br in the gaseous, liquid and solid state. XAS spectrum for gaseous Br_2 and HBr have for instance been reported by D'Angelo et al. (1993). Gaseous Br_2 is characterized by a sharp pre-edge peak around 15 eV below the absorption edge (~13,465 eV), the absence of a white line and well-defined EXAFS oscillations, due to the presence of a 'heavy' Br nearest-neighbour. None of these features is present in our high P-T spectra (Fig. 5) and the formation of Br_2 in the MVPs is hence discarded. In comparison, gaseous HBr displays no pre-edge peak and a featureless EXAFS part, due to the weak scattering power of the neighbouring hydrogen atom. While there is a small white line located around 13,480 eV, its amplitude remains significantly lower than that we observe in the MVP, suggesting that the Br specie present in the MVP is not HBr. Instead, we find the XANES spectrum of Br in the MVP to remain quite similar to that of Br in the starting aqueous solution (Fig. 5), where Br is a hydrated ion, surrounded by six to eight H_2O molecules (Antalek et al., 2016; Louvel et al., 2020a). The intensity of the white line is however reduced compared to that of aqueous Br, which may suggest dehydration of the Br ion to some extent forming species as $[Br(H_2O)_n]^-$ ($n < 6$). Such temperature induced dehydration of the Br ion is further supported by the fact that the amplitude of the white line continues to decrease from 650 to 800 °C while the density of the MVPs decreases from around 0.32 to 0.23 g·cm^{-3} (pure H_2O density). Another possibility is that the change in the XANES spectra results partly from ion association in the low-density 'gas-like' MVPs, with the formation of neutral species as $[NaBr(H_2O)_x]$. Ion association and the stabilization of neutral compounds rather than ionic species is indeed expected in high-temperature low-density fluids due to the strong decrease of the dielectric constant with increasing temperature and decreasing density. While Na-Cl ion association has been suggested to some extent in supercritical water from theoretical calculations (Cui and Harris, 1994), it has, to the best of our knowledge, only been described spectroscopically in fluids of intermediate to high-density ($\rho > 0.45$ g·cm^{-3}) (Elbers et al., 2021). Although we cannot yet distinguish whether Br is present as

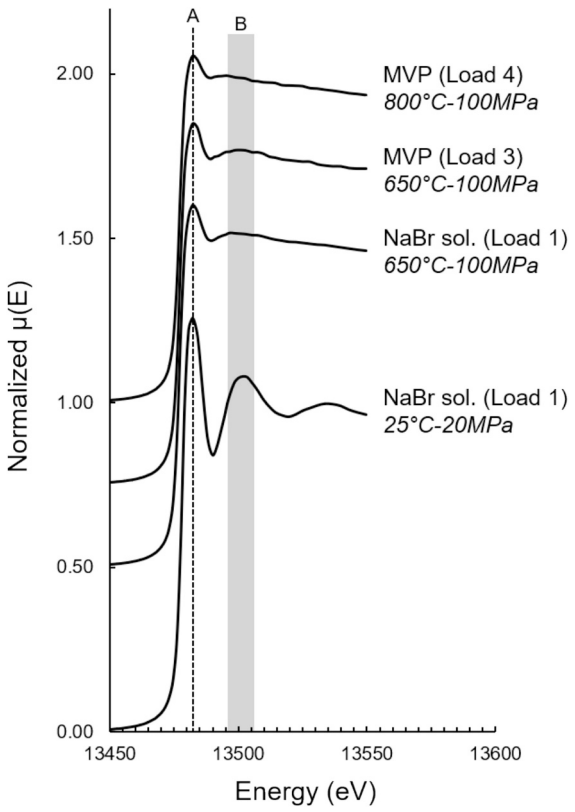

Fig. 5. Bromine XAS spectra collected in the NaBr solution (Load 1) and Br-bearing MVPs (Loads 3 and 4) at room conditions and 650–800 °C and 100 MPa. (A) and (B) underline the white line and first oscillation position, respectively.

hydrated $[Br(H_2O)_n]^-$ ($n < 6$), reactive Br^+OH^- or neutral [NaBr $(H_2O)_x$] species based on our preliminary in-situ observations, it is obvious from the XANES spectra that HBr is not the main Br specie in our H_2O-NaBr low-density fluids. We also discard the potential formation of reactive Br species involving O (e.g., BrOH) as the change in oxidation state from −1 to +1 would likely give rise to differences in the XAS spectra. While such species have been reported in volcanic plumes, they are expected to form from the fast high-temperature oxidation of HBr in the volcanic gas-air mixture (Rüdiger et al., 2017). We thus suggest that while Br may be transported as hydrated species in shallow degassing systems, HBr formation should be expected closer to the surface in natural systems, after significant expansion of the MVP to the gaseous state (density < 0.1 g·cm^{-3}).

Although Br speciation in the melt could not investigated in-situ, we expect Br to be found in similar alkali- and alkaline earth-rich domains as previously reported in high P-T haplosilicate melts and natural volcanic glasses (Louvel et al., 2020a, 2020b; Cochain et al., 2015).

4.2. Sr in the haplogranite-MVP system

The initial concentration of Sr in the Hpg_ML4 glass could be calculated from XAS spectra collected at room conditions, taking into account a density for the dry glass of 2.24 g·cm^{-3}. They are around 1.03 wt% for a nominal input of 1 wt%. Upon heating to 650 and 800 °C, we observe no Sr absorption edge in the MVP, suggesting that Sr concentration were below the 10 ppm level in this phase (fluorescence detection limit based on previous studies on hydrothermal fluids, e.g., Louvel et al., 2017) and that Sr largely remains in the melt phase up to high P-T conditions.

Using melt densities of 2.1–2.18 g·cm^{-3} for an haplogranite melt containing 5 to 6 wt% dissolved H_2O (Ochs and Lange, 1999), Sr concentrations calculated from the in-situ XAS spectra collected in the melt are 1.045 ± 0.015 and 0.998 ± 0.015 wt% at 650 and 800 °C, respectively. These calculated values are in good agreement with the EPMA analysis of the melt recovered from Load 4 (i.e., quenched at 800 °C) that suggests an average of 1.06 ± 0.06 wt% Sr ($n = 9$ – see Supplementary Materials for all EPMA analyses). The stable Sr concentration in the Hpg4Sr melt and the absence of Sr signal in the MVPs are in line with the low $D_{Sr}^{fluid/melt} = 0.006$ reported by Borchert et al. (2009) from in-situ SXRF measurements at 750 °C and 360 MPa in the HDAC.

The speciation of Sr in the high P-T melt could also be evaluated from the in-situ XAS. The XANES spectra collected in the Sr-doped haplogranite glass under room conditions resemble the high-resolution HERFD-XAS spectra reported by Borchert et al. (2014) for peralkaline granites, where Sr was suggested to be present as distorted SrO_6 clusters with Sr-O average distance of 2.62 Å. They are characterized by a relatively broad white line that peaks around 16,121 eV and display a large shoulder around 16,130 eV. With melting at 800 °C and 100 MPa, this shoulder is found to largely disappear, while the EXAFS part of the spectra considerably flattens (Fig. 6). These changes are associated with a slight shift in the 2nd EXAFS oscillation from ~3.88 to 4 Å^{-1} and the reduction of the amplitude of the 3rd EXAFS oscillation localized around 5.5 Å^{-1} (Fig. 6B). Previous EXAFS analysis of Sr local environment in silicate glasses suggest Sr is coordinated to 5 to 8 oxygen atoms located at an average of 2.5–2.73 Å (Kohn et al., 1990; McKeown et al., 2003; Pohlenz et al., 2018). Here, the best EXAFS fit are obtained for 5.0 ± 0.5 oxygen atoms located at an average of 2.53 ± 0.03 Å from the central strontium atom (Fig. 6B – Table S2 in Supp. Mat.). Despite the shape and position differences in XANES and EXAFS oscillations, we do not find significant differences in the fitted coordination number and bond distance for the high P-T melt: the best fit is obtained for Sr surrounded by 5.1 ± 0.9 oxygens at an average distance of 2.51 ± 0.03 Å. We however note a strong decrease of the overall quality of the fit and larger uncertainties on fitted structural parameters (Table S2 in Supp. Mat.). High temperature conditions and melting of the glass indeed result in further disorder in the structure and an overall damping and larger anharmonicity of the EXAFS signal, further enhanced in the case of Sr than other trace elements (Pohlenz et al., 2018; Wilke, 2018). The fitted coordination number and bond distance differ slightly from those previously reported for peralkaline melts by Pohlenz et al. (2018) (i.e., 7 oxygens at 2.60 Å). While we cannot discard these small discrepancies arise from the lower quality of the high P-T fit, we believe differences in the high P-T melts composition could also explain structural differences, as Pohlenz et al.'s starting materials were extremely peralkaline (Na_2O ~ 18 wt%)

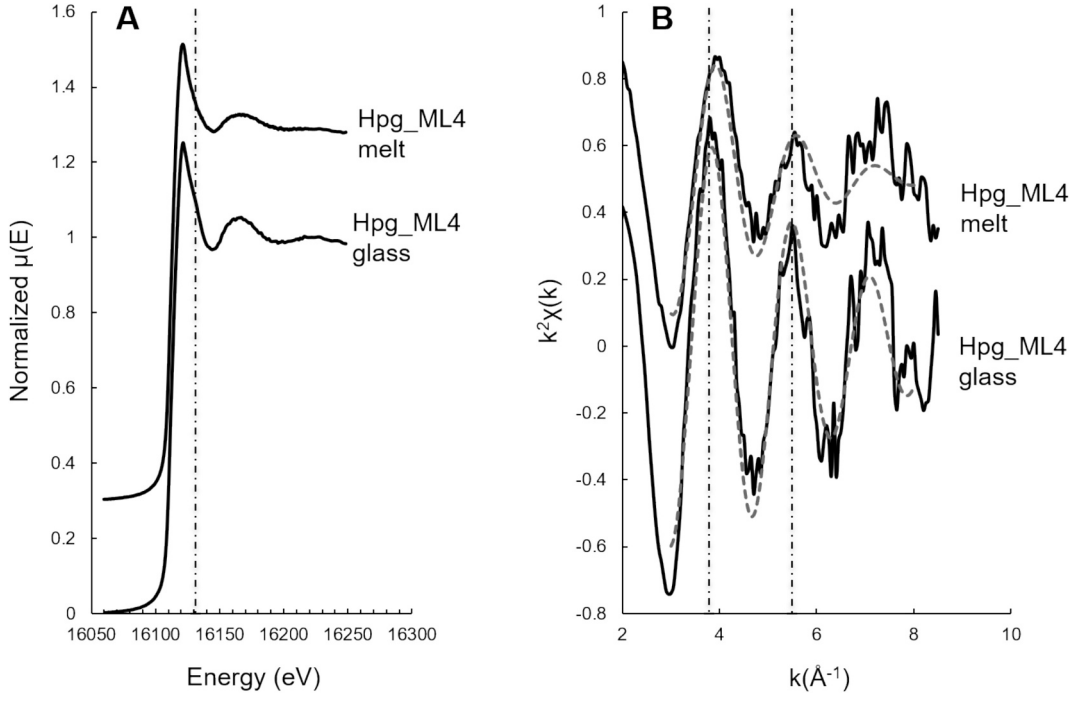

Fig. 6. Strontium K-edge XANES (A) and k^2-weighted EXAFS oscillations (B) collected in the Hpg4Sr glass and high P-T melt in Load 4 (800 °C and 100 MPa). The vertical black dashed lines underline differences between glass and melt. The grey dashed lines on (B) are the EXAFS fits.

and Si-poor (SiO_2 ~ 58 wt%) compared to our Hpg_ML4 melt.

5. Conclusions

The presented experimental results constitute the first steps towards the in-situ characterization of MVPs and their role in magmatic-hydrothermal and volcanic processes. While the attainment of equilibrium still needs to be tested systematically for different elements over long time periods (9–12 h) and the set-up is yet to be tested to reach temperature conditions necessary to melt andesitic and basaltic compositions (1000–1200 °C), we expect the T-IHPV to offer new opportunities to study the distribution and speciation of C-O-H-N-S volatiles, but also of various metals (with 22 < Z) between MVPs and melts or other biphasic high-temperature systems (i.e., brine-vapour separation). A total of 8 transparent autoclaves are now available at the Institut des Sciences de la Terre d'Orleans (ISTO, Orleans, France), Institut Neel and FAME and FAME-UHD beamlines (ESRF synchrotron, Grenoble, France). Current and future experimental developments include their coupling to 1) Raman to allow for the detection and quantification of various volatiles species in supercritical fluids and gases, including CH_4, CO, CO_2, H_2S, SO_2 or NH_4 (Louvel et al., 2015, 2017), 2) high-resolution crystal analyzer spectrometers (CAS) for high energy resolution fluorescence XAS measurements (HERFD-XAS) to refine the nature and geometry of metallic complexes in hydrothermal fluids and MVPs (e.g., Pokrovski et al., 2022) and 3) X-ray diffraction to study hydrothermal and gaseous alteration of natural rocks.

CRediT authorship contribution statement

Marion Louvel: Writing – original draft, Investigation, Conceptualization. **Denis Testemale:** Writing – review & editing, Methodology, Investigation, Conceptualization. **Alain Prat:** Methodology, Conceptualization. **Eric Lahera:** Methodology, Conceptualization. **William Del-Net:** Data curation. **Aneta Slodczyk:** Writing – review & editing, Investigation. **Benjamin Langerome:** Writing – review & editing, Visualization. **Remi Champallier:** Writing – review & editing, Investigation. **Richard Brooker:** Investigation. **Anita Cadoux:** Writing – review & editing, Investigation. **Jasper Berndt:** Writing – review & editing, Investigation. **Jean-Louis Hazemann:** Writing – review & editing, Methodology, Conceptualization.

Declaration of competing interest

The authors declare that they have no known competing financial interests or personal relationships that could have appeared to influence the work reported in this paper.

Acknowledgments

The authors acknowledge Equipex Planex (ANR-11-EQPX-0036) funding for the design, construction and implementation of the transparent IHPV and associated equipment. The Soleil (CRG) and ESRF synchrotrons are acknowledged for beamtime allocation. The authors wish to thank O. Proux and I. Kieffer from Univ. Grenoble Alpes –OSUC for extra support during the in-situ XAS measurements. B. Scaillet from ISTO is also thanked for leading the Equipex Planex project.

Appendix A. Supplementary data

Supplementary data to this article can be found online at https://doi.org/10.1016/j.jvolgeores.2025.108381.

Data availability

Data will be made available on request.

References

Alex, A., Zajacz, Z., 2020. A new method to quantitatively control oxygen fugacity in externally heated pressure vessel experiments. Eur. J. Mineral. 32, 219–234.
Alletti, M., Baker, D.R., Scaillet, B., Aiuppa, A., Moretti, R., Ottolini, L., 2009. Chlorine partitioning between a basaltic melt and H2O-CO2 fluids at Mount Etna. Chem. Geol. 263, 37–50.
Antalek, M., Pace, E., Hedman, B., Hodgson, K.O., Chillemi, G., Benfatto, M., Sarangi, R., Frank, P., 2016. Solvation structure of the halides from x-ray absorption spectroscopy. J. Chem. Phys. 145, 044318-1–1–1–15.
Audetat, A., Edmonds, M., 2020. Magmatic-hydrothermal fluids. Elements 16, 401–406.
Bassett, W.A., 2003. High pressure-temperature aqueous systems in the hydrothermal Diamond anvil cell (HDAC). Eur. J. Mineral. 15, 773–780.
Bassett, W.A., Shen, A.H., Bucknum, M., Chou, I.-M., 1993. Rev. Sci. Instrum. 64, 2340–2345.
Berndt, J., Liebske, C., Holtz, F., Freise, M., Nowak, M., Ziegenbein, D., Hurkuck, W., Koepke, J., 2002. A combined rapid-quench and H2-membrane setup for internally heated pressure vessels: description and application for water solubility in basaltic melts. Am. Mineral. 87, 1717–1726.
Borchert, M., Wilke, M., Schmidt, C., Rickers, K., 2009. Partitioning and equilibration of R band Sr between silicate melts and aqueous fluids. Chem. Geol. 259, 39–47.
Borchert, M., Wilke, M., Schmidt, C., Kvashnina, K., Jahn, S., 2014. Strontium complexation in aqueous solutions and silicate glasses: insights from high energy-resolution fluorescence detection X-ray spectroscopy and ab-initio modelling. Geochim. Cosmochim. Acta 142, 535–552.
Borchert, M., Wilke, M., Schmidt, C., Rickers, K., 2010. Rb and Sr partitioning between haplogranitic melts and aqueous solutions. Geochim. Cosmochim. Acta 74, 1057–1076.
Botcharnikov, R., Freise, M., Holtz, F., Behrens, H., 2005. Solubility of C-O-H mixtures in natural melts: new experimental data and application range of recent models. Annals of Geophysics 48, 633–646.
Bruyere, R., Prat, A., Goujon, C., Hazemann, J-L., 2008. A new pressure regulation device using high pressure isolation valves. J. Phys. Conf. Ser. 121, 122003.
Bureau, H., Keppler, H., Metrich, N., 2000. Volcanic degassing of bromine and iodine: experimental fluid/melt partitioning data and applications to stratospheric chemistry. Earth Planet. Sci. Lett. 183, 51–60.
Burgisser, A., Alletti, M., Scaillet, B., 2015. Simulating the behaviour of volatiles belonging to the C-O-H-S system in silicate melts under magmatic conditions with the software D-Compress. Comput. Geosci. 79, 1–14.
Burnham, C.W., Jahns, R.H., 1962. A method for determining solubility of water in silicate melts. Am. J. Sci. 260, 721–745.
Burnham, C.W., 1962. Large volume apparatus for hydrothermal investigations to 10,000 bars and 1500°C (abs). Amer. Ceram. Soc. Program, Seattle, Washington.
Burnham, C.W., Holloway, J.R., Davis, N.F., 1969. The specific volume of water in the range 1000 to 8900 bars, 20 to 900C. Am. J. Sci. 267A, 70–95.
Cadoux, A., Iacono-Marziano, G., Scaillet, B., Aiuppa, A., Mather, T.A., Pyle, D.M., Deloule, E., Gennaro, E., Paonita, A., 2018. The role of melt composition on aqueous fluid vs. silicate melt partitioning of bromine in magmas. Earth Planet. Sci. Lett. 498, 450–463.
Cassidy, M., Iveson, A.A., Humphreys, M.C., Mather, T.A., Helo, C., Castro, J.M., Ruprecht, P., Pyle, D.M., EIMF, 2022. Experimentally derived F, Cl, and Br fluid/melt partitioning of intermediate to silicic melts in shallow magmatic systems. Am. Mineral. 107 (10), 1825–1839.
Caumon, M.-C., Robert, P., Laverret, E., Tarantola, A., Randi, A., Pironon, J., Dubessy, J., Girard, J.-P., 2014. Determination of methane content in NaCl-H2O fluid inclusions by Raman spectroscopy. Calibration and application to the external part of the Central Alps (Switzerland). Chem. Geol. 378, 52–61.
Chiodini, G., et al., 2017. Fumarolic tremor and geochemical signals during a volcanic unrest. Geology 45, 1131–1134. https://doi.org/10.1130/G39447.1.
Chou, I.-M., 2012. Optical cells with fused sílica windows for the study of geological fluids. In: European Mineralogical Union Notes in Mineralogy, vol.12, pp. 227–247. Chapter 6.
Cochain, B., Sanloup, C., de Grouchy, C., Crepisson, C., Bureau, H., Leroy, C., Kantor, I., Irifune, T., 2015. Bromine speciation in hydrous silicate melts at high pressure. Chem. Geol. 404, 18–26.
Cui, S.T., Harris, J.G., 1994. Ion association and liquid structure in supercritical water solutions of sodium chloride: a microscopic view from molecular dynamics simulations. Chem. Eng. Sci. 49, 2749–2763.
D'Angelo, P., Di Cicco, A., Filipponi, A., Pavel, N.V., 1993. Double-electron excitation channels at the Br K-edge of HBr and Br2. Phys. Rev. A 47, 2055–2063.
Driesner, T., 2007. The system H2O-NaCl. Part II: correlations for molar volume, enthalpy, and isobaric heat capacity from 0 to 1000°, 0 to 5000 bar, and 0 to 1 XNaCl. Geochim. Cosmochim. Acta 71, 4902–4919.
Edmonds, M., Wallace, P.J., 2017. Volatiles and exsolved vapors in volcanic systems. Elements 13, 29–34.
Elbers, M., Schmidt, C., Sternemann, C., Sahle, C.J., Jahn, S., Albers, C., Sakrowski, R., Gretarsson, H., Sundermann, M., Tolan, M., Wilke, M., 2021. Ion association in hydrothermal aqueous NaCl solutions: implications fort he microscopic structure of supercritical water. Physical Chemicstry, Chemical Physics 23, 14845.
Etschmann, B.E., Liu, W., Testemale, D., Muller, H., Rae, N.A., Proux, O., Hazemann, J.L., Brugger, J., 2010. An in situ XAS study of copper(I) transport as hydrosulfide complexes in hydrothermal solutions (25–592 C, 180–600 bar): speciation and solubility in vapor and liquid phases. Geochim. Cosmochim. Acta 74, 4723–4739.
Flematakis, S., Berndt, J., Klemme, S., Genske, F., Cadoux, A., Louvel, M., Rohrbach, A., 2020. An improved electron microprobe method for the analysis of halogens in natural silicate glasses. Microsocpy and Microanalysis 26, 857–866.

Frank, M.R., Simon, A.C., Pettke, T., Candela, P.A., Piccoli, P.M., 2011. Gold and copper partitioning in magmatic-hydrotehrmal systems at 800C and 100MPa. Geochim. Cosmochim. Acta 75, 2470–2482.
Gennaro, E., Iacono-Marziano, G., Paonita, A., Rotolo, S.G., Martel, C., Rizzo, A.L., Pichavant, M., Liotta, M., 2019. Melt inclusions track melt evolution and degassing of Etnean magmas in the last 15ka. Lithos 324–325, 716–732.
Gion, A.M., Gaillard, F., Freslon, N., Erdmann, S., Di Carlo, I., 2022. A method for the direct analysis of quenched, magmatic-hydrothermal fluids recovered from high-pressure, high-temperature experiments. Chem. Geol. 609, 121061.
Gooding, J.L., Muenow, D.W., 1976. Activated release of alkalis during the vesiculation of molten basalts under high vacuum: implications for lunar volcanism. Geochim. Cosmochim. Acta 40, 675–686.
Guan, Q., Mei, Y., Estchmann, B., Testemale, D., Louvel, M., Brugger, J., 2020. Yttrium complexation and hydration in chloride-rich hydrothermal fluids: a combined ab initio molecular dynamics and in situ X-ray absorption spectroscopy study. Geochimica et Cosmochimca Acta 281, 168–189.
Guo, H., Audetat, A., 2017. Transfer of volatiles and metals from mafic to felsic magmas in composite magma chambers: an experimental study. Geochim. Cosmochim. Acta 198, 360–378.
Guo, H., Audetat, A., 2018. Gold diffusion into and out of quartz-hosted fluid inclusions during re-equilibration experiments at 600–800°C and 2kbar. Chem. Geol. 476, 1–10.
Hack, A.C., Mavrogenes, J.A., 2006. A synthetic fluid inclusion study of copper solubility in hydrothermal brines from 525 to 725°C and 0.3 to 1.7GPa. Geochim. Cosmochim. Acta 70, 3970–3985.
Hashimoto, A., 1992. The effect of H2O gas on volatilies of planet-forming major elements: I. Experimental determination of thermodynamic properties of Ca-, Al-, and Si-hydroxide gas molecules and its application to the solar nebula. Geochim. Cosmochim. Acta 56, 511–532.
Heinrich, C.A., Pettke, T., Halter, W.E., Aigner-Torres, M., Audetat, A., Gunther, D., Hattendorf, B., Bleiner, D., Guillong, M., Horn, I., 2003. Quantitative multi-element analysis of minerals, fluid and melt inclusions by laser-ablation inductively-coupled plasma mass-spectrometry. Geochim. Cosmochim. Acta 67, 3473–3496.
Henley, R.W., Seward, T.M., 2018. Gas-solid reactions in arc volcanoes: ancient and modern. Rev. Mineral. Geochem. 84, 309–349.
Holloway, J.R., 1971. Internally heated pressure vessels. In: Ulmer, G.C. (Ed.), Research Techniques for High Temperature and Pressure. Springer Verlag, New York, pp. 217–258.
Holloway, J.R., Dixon, J.E., Pawley, A.R., 1992. An internally heated, rapid-quench, high-pressure vessel. Am. Mineral. 77, 643–646.
Holtz, F., Behrens, H., Dingwell, D.B., Johannes, W., 1995. H2O solubility in haplogranitic melts: compositional, pressure, and temperature dependence. Am. Mineral. 80, 94–108.
Hurtig, N.C., Migdisov, A.A., Williams-Jones, A.E., 2021. Are vapour-like fluids viable ore fluids for Cu-Au-Mo porphyry ore formation? Econ. Geol. 116, 1599–1624.
Iveson, A.A., Webster, J.D., Rowe, M.C., Neill, O.K., 2017. Major element and halogen (F, Cl) mineral-melt-fluid partitioning in hydrous rhyodacitic melts at shallow crustal conditions. J. Petrol. 58, 2465–2492.
Iveson, A.A., Webster, J.D., Rowe, M.C., Neill, O.K., 2019. Fluid-melt trace-element partitioning behaviour between evolved melts and aqueous fluids: Experimental constraints on the magmatic-hydrothermal transport of metals. Chem. Geol. 516, 18–41.
Keppler, H., Cialdella, L., Couffignal, F., Wiedenbeck, M., 2022. The solubility of N2 in silicate melts and nitrogen partitioning between upper mantle minerals and basalt. Contrib. Mineral. Petrol. 177, 83.
Kohn, S.C., Charnock, J.M., Henderson, C.M.B., Greaves, G.N., 1990. The structural environments of trace elements in dry and hydrous silicate glasses; a manganese and strontium K-edge X-ray absorption spectroscopic study. Contrib. Mineral. Petrol. 105, 359–368.
Lecumberri-Sanchez, P., Luo, M., Steele-MacInnis, M., Runyon, S.E., Sublett Jr., M., Klyukin, Y., Bodnar, R.J., 2020. Synthetic fluid inclusions XXII: Properties of H2O-NaCl±KCl fluid inclusions trapped under vapour- and salt-saturated conditions with emphasis on the effect of KCl on phase equilibria. Geochim. Cosmochim. Acta. https://doi.org/10.1016/j.gca.2019.12.018.
Lemke, K.H., Seward, T.M., 2018. Molecular clusters and solvation in volcanic and hydrothermal vapors. Rev. Mineral. Geochem. 84, 57–83.
Lesne, P., Scaillet, B., Pichavant, M., Beny, J.-M., 2011. The carbon dioxide solubility in alkali basalts: an experimental study. Contrib. Mineral. Petrol. 162, 153–168.
Lesne, P., Scaillet, B., Pichavant, M., 2015. The solubility of sulfur in hydrous basaltic melts. Chem. Geol. 418, 104–116.
Li, J., Bassett, W.A., Chou, I.-M., Ding, X., Li, S., Wang, X., 2016. An improved hydrothermal diamond anvil cell. Rev. Sci. Instrum. 87, 053108.
Louvel, M., Sanchez-Valle, C., Malfait, W.J., Cardon, H., Testemale, D., Hazemann, J.L., 2014. Constraints on the mobilization of Zr in magmatic-hydrothermal processes in subduction zones from in situ fluid-melt partitioning experiments. Am. Mineral. 99, 1616–1625.
Louvel, M., Bordage, A., Da Silva-Cadoux, C., Testemale, D., Lahera, E., Del Net, W., Geaymond, O., Dubessy, J., Argoud, R., Hazemann, J.L., 2015. A high-pressure high-temperature setup for in situ Raman spectroscopy of supercritical fluids. J. Mol. Liq. 205, 54–60.
Louvel, M., Bordage, A., Tripoli, B., Testemale, D., Hazemann, J.-L., Mavrogenes, J., 2017. Effect of S on the aqueous and gaseous transport of Cu in porphyry and epithermal systems: constraints from in situ XAS measurements up to 600 C and 300 bars. Chem. Geol. 466, 500–511.
Louvel, M., Sanchez-Valle, C., Malfait, W.J., Pokrovski, G.S., Borca, C.N., Grolimund, D., 2020a. Bromine speciation and partitioning in slab-derived aqueous fluids and silicate melts and implications for halogen transfer in subduction zones. Solid Earth 11, 1145–1161.
Louvel, M., Cadoux, A., Brooker, R.A., Proux, O., Hazemann, J.L., 2020b. New insights on Br speciation in volcanic glasses and structural controls on halogen degassing. Am. Mineral. 105, 795–802.
Luth, W.C., Tuttle, O.F., 1949. Externally heated cold-seal pressure vessels for use to 10,000 bars and 750°C. Am. Mineral. 48, 1401–1403.
Mavrogenes, J.A., Bodnar, R.J., 1994. Hydrogen movement into and out of fluid inclusions in quartz: experimental evidence and geologic implications. Geochim. Cosmochim. Acta 58, 141–148.
McKeown, D.A., Kot, W.K., Pegg, I.L., 2003. X-ray absorption studies of the local strontium environments in borosilicate waste glasses. J. Non Cryst. Solids 317, 290–300.
Meschter, P.J., Opila, E.J., Jacobson, N.S., 2013. Water vapor-mediated volatilization of high-temperature materials. Annu. Rev. Mat. Res. 43, 559–588.
Metrich, N., Wallace, P.J., 2008. Volatile abundances in basaltic magmas and their degassing paths tracked by melt inclusions. Reviews in Mineralogy and Geochemsitry 69, 363–402.
Moretti, R., Arienzo, I., Civetta, L., Orsi, G., Papale, P., 2013. Multiple magma degassing sources at an explosive volcano. Earth Planet. Sci. Lett. 367, 95–104.
Moussallam, Y., Morizet, Y., Massuyeau, M., Laumonier, M., Gaillard, F., 2015. CO2 solubility in kimberlite melts. Chem. Geol. 418, 198–205.
Myers, D.L., Jacobson, N.S., 2019. Identification of volatile metal hydroxides with free jet expansion sampling mass spectrometry. Calphad 65, 73–78.
Mysen, B., 2010. Structure of H2O-saturated peralkaline aluminosilicate melt and coexisting aluminosilicate-saturated aqueous fluid determined in-situ to 800C and ~800MPa. Geochim. Cosmochim. Acta 74, 4123–4139.
Nekvasil, H., DiFrancesco, N.J., Rogers, A.D., Coraor, A.E., King, P.L., 2019. Vapor-deposited minerals contributed to the Martian surface during magmatic degassing. JGR Planets 124, 1592–1617.
Ni, H., Keppler, H., 2013. Carbon in silicate melts. Rev. Mineral. Geochem. 75, 251–287.
Ochs, F.A.I.I.I., Lange, R.A., 1999. The density of hydrous magmatic liquids. Science 283, 1314–1317.
Oppenheimer, C., Fischer, T.P., Scaillet, B., 2014. Volcanic degassing: process and impact. In: Treatise on Geochemistry, 2nd edition 4, pp. 111–179.
Pohlenz, J., Rosa, A.D., Mathon, O., Pascarelli, S., Belin, S., Landrot, G., Murzin, V., Veligzhanin, A., Shiryaev, A., Irifune, T., Wilke, M., 2018. Structural controls of CO2 on Y, La, and Sr incorporation in sodium-rich silicate-carbonate melts by in-situ high P-T EXAFS. Chem. Geol. 486, 1–15.
Pokrovski, G.S., Borisova, A.Y., Bychkov, A.Y., 2013. Speciation and transport of metals and metalloids in geological vapors. Rev. Mineral. Geochem. 76, 165–218.
Pokrovski, G.S., Desmale, E., Laskar, C., Bazarkina, E.F., Testemale, D., Hazemann, J.-L., Vuilleumier, R., Seitsonen, A.P., Ferlat, Saitta, A.M., 2022. Gold speciation in hydrothermal fluids revealed by in-situ high energy resolution X-ray absorption spectroscopy. Am. Mineral. 107, 369–376.
Proux, O., Biquard, X., Lahera, E., Menthonnex, J.-J., Prat, A., Ulrich, O., Soldo, Y., Trévisson, P., Kapoujvan, G., Perroux, G., Taunier, P., Grand, D., Jeantet, P., Deleglise, M., Roux, J.-P., Hazemann, J.-L., 2005. FAME: a new beamline for X-ray absorption investigations of very-diluted systems of environmental, material and biological interests. Phys. Scr. 115 (2005), 970–973.
Ravel, B., Newville, M., 2005. Athena, Artemis, Hephaestus: data analysis for X-ray absorption spectroscopy using IFEFFIT. J. Synchrotron Radiat. 12, 537–541.
Renggli, C.J., Klemme, S., 2020. Experimental constraints on metal transport in fumarolic gases. J. Volcanol. Geotherm. Res. 400, 106929.
Rüdiger, J., Bobrowski, N., Liotta, M., Hoffmann, T., 2017. Development and application of a sampling method for the determination of reactive halogen species in volcanic gas emissions. Anal. Bioanal. Chem. 409, 5975–5985.
Scaillet, B., Pichavant, M., 2005. A model of sulphur solubility for hydrous mafic melts: application to the determination of magmatic fluid compositions of Italian volcanoes. Ann. Geophys. 48, 671–698.
Scaillet, B., Pichavant, M., Roux, J., Humbert, G., Lefevre, A., 1992. Improvments of the Shaw membrane technique for measurements and control of fH2 at high temperatures and pressures. Am. Mineral. 77, 647–655.
Schienbein, P., Marx, D., 2020. Assessing the properties of supercritical water in terms of structural dynamics and electronic polarization effects. Phys. Chem. Chem. Phys. 22, 10462–10479.
Schmidt, C., 2018. Formation of hydrothermal tin deposits: Raman spectroscopic evidence for an important role of aqueous Sn(IV) species. Geochim. Cosmochim. Acata 220, 499–511.
Signorelli, S., Carroll, M.R., 2002. Experimental study of Cl solubility in hydrous alkaline melts: constraints on the theoretical maximum amount of Cl in trachytic and phonolitic melts. Contrib. Mineral. Petrol. 143, 209–218.
Simon, A.C., Frank, M.R., Pettke, T., Candela, P.A., Piccoli, P.M., Heinrich, C.A., 2005. Gold partitioning in melt-vapor-brine systems. Geochim. Cosmochim. Acta 69, 3321–3335.
Solferino, G., Anderson, A.J., 2012. Thermal reduction of molybdite and hematite in water and hydrogen peroxide-bearing solutions: Insights on redox conditions in hydrothermal diamond anvil cell (HDAC) experiments. Chem. Geol. 322-323, 215–222.
Sterner, S.M., Bodnar, R.J., 1984. Synthetic fluid inclusions in natural quartz I. Compositional types synthesized and applications to experimental geochemistry. Geochim. Cosmochim. Acta 48, 2659–2668.
Symonds, R.B., Reed, M.H., 1993. Calculation of multicomponent chemical equilibria in gas - solid -liquid systems; calculation methods, thermochemical data, and applications to studies of high -temperature volcanic gases with examples from Mount St. Helens. Am. J. Sci. 293, 758–864.

Tattitch, B.C., Blundy, J.D., 2017. Cu-Mo partitioning between felsic melts and saline-aqueous fluids as a function of XNaCleq, fO2 and FS2. Am. Mineral. 102, 1987–2006.
Tattitch, B.C., Candela, P.A., Piccoli, P.M., Bodnar, R.J., 2014. Copper partitioning between felsic melt and CO2-H2O bearing saline fluids. Geochim. Cosmochim. Acta 148, 81–99.
Tattitch, B.C., Chelle-Michou, C., Blundy, J., Loucks, R.R., 2021. Chemical feedbacks during magma degassing control chlorine partitioning and metal extraction in volcanic arcs. Nat. Commun. 12, 1774. https://doi.org/10.1038/s41467-021-21887-w.
Testemale, D., Argoud, R., Geaymond, O., Hazemann, J.-L., 2005. High pressure/high temperature cell for X-ray absorption and scattering techniques. Review of Scientific Instruments 76, 043905.
Thompson, M.A., Telus, M., Schaefer, L., Fortney, J.J., Joshi, T., Lederman, D., 2021. Composition of terrestrial exoplanet atmospheres from meteorite outgassing experiments. Nature Astronomy 5, 575–585.
Von Glasow, R., Bobrowski, N., Kern, C., 2009. The effects of volcanic eruptions on atmospheric chemistry. Chem. Geol. 263, 131–142.
Waelkens, C.M., Stix, J., Montelone, B., Burckel, P., 2021. Efficient release of bromine by super-eruptions. Geology 49, 1416–1420.
Wagner, W., Pruss, A., 2002. The IAPWS formulation 1995 for the thermodynamic properties of ordinary water substance for general and scientific use. J. Phys. Chem. Ref. Data 31 (2), 387–535. https://doi.org/10.1063/1.1461829.
Webster, J.D., 1992. Water solubility and chlorine partitioning in Cl-rich granitic systems: Effects of melt composition at 2kbar and 800°C. Geochim. Cosmochim. Acta 56, 679–687.
Webster, J.D., 1997. Exsolution of magmatic volatile phases from Cl-enriched mineralizing granitic magmas and implications for ore metal transport. Geochim. Cosmochim. Acta 61, 1017–1029.
Webster, J.D., Botcharnikov, R.E., 2011. Distribution of sulfur between melt and fluid in S-O-H-C-Cl-bearing magmatic systems at shallow crustal pressures and temperatures. Rev. Mineral. Geochem. 73, 247–283.
Webster, J.D., Holloway, J.R., 1988. Experimental constraints on the partitioning of Cl between topaz rhyolite melt and H2O and H2O+CO2 fluids: new implications for granitic differentiation and ore deposition. Geochim. Cosmochim. Acta 52, 2091–2105.
Webster, J.D., Holloway, J.R., Hervig, R.L., 1989. Partitioning of lithophile trace elements between H2O and H2O+CO2 fluids and topaz rhyolite melt. Econ. Geol. 84, 116–134.
Webster, J.D., Kinzler, R.J., Mathez, E.A., 1999. Chloride and water solubility in basalt and andesite melts and implications for magmatic degassing. Geochim. Cosmochim. Acta 63, 729–738.
Webster, J.D., Sintoni, M.F., De Vivo, B., 2009. The partitioning behavior or Cl, S, and H2O in aqueous vapor-±saline-liquid saturated phonolotic and trachytic melts at 200MPa. Chem. Geol. 263, 19–36.
Webster, J.D., Goldoff, B., Sintoni, M.F., Shimizu, N., De Vivo, B., 2014. C-O-H-Cl-S-F volatiles solubilities, partitioning, and mixing in phonolitic-trachytic melts and aqueous-carbonic vapor±saline liquid at 200 MPa. J. Petrol. 55, 2217–2248.
Wilke, M., 2018. X-ray absorption spectroscopy measurements. In: Magmas Under Pressure, pp. 155–178.
Wilke, M., Klimm, K., Kohn, S.C., 2011. Spectroscopic studies on sulfur speciation in synthetic and natural glasses. Rev. Mineral. Geochem. 73, 41–78.
William, D.W., 1968. Improved cold seal pressure vessels to operate to 1100°C at 3 kilobars. Am. Mineral. 53, 1765–1769.
Williams-Jones, A.E., Heinrich, C.A., 2005. Vapor transport of metals and the formation of magmatic-hydrothermal ore deposits. Econ. Geol. 100, 1287–1312.
Zajacz, Z., 2015. The effect of melt composition on the partitioning of oxidized sulfur between silicate melts and magmatic volatiles. Geochim. Cosmochim. Acta 158, 223–244.
Zajacz, Z., Candela, P.A., Piccolo, P.M., 2017. The partitioning of Cu, Au and Mo between liquid and vapor at magmatic temperatures and its implications for the genesis of magmatic-hydrothermal ore deposits. Geochim. Cosmochim. Acta 207, 81–101.
Zajacz, Z., Hanley, J.J., Heinrich, C.A., Halter, W.E., Guillong, M., 2009. Diffusive reequilibration of quartz-hosted silicate melt and fluid inclusions: are all metal concentrations unmodified? Geochim. Cosmochim. Acta 73, 3013–3027.
Zajacz, Z., Seo, J.-H., Candela, P.A., Piccoli, P.M., Heinrich, C.A., Guillong, M., 2010. Alkali metals control the release of gold from volatile-rich magmas. Earth Planet. Sci. Lett. 297, 50–56.
Zajacz, Z., Candela, P.A., Piccoli, P.M., Sanchez-Valle, C., 2012. The partitioning of sulfur and chlorine between andesite melts and magmatic volatiles and the exchange coefficients of major cations. Geochim. Cosmochim. Acta 89, 81–101.